Dynamic switching of the plasmonic beam on the spiral bull's eye structure[◊]

Seung-Yeol Lee, Il-Min Lee, Junghyun Park, Chi-Young Hwang, and Byoungho Lee[*]

National Creative Research Center for Active Plasmonics Application Systems

Inter-University Semiconductor Research Center and School of Electrical Engineering

Seoul National University, Gwanak-Gu Gwanakro 599, Seoul 151-744, Korea

[*]*Corresponding author: byoungho@snu.ac.kr*

A polarization dependent switchable plasmonic beaming structure composed of metallic hole surrounded by double spiral dielectric gratings is proposed. The main mechanism of the proposed structure is based on the angular momentum change of surface plasmon caused by the spiral geometry. On- and off-states of the proposed device are determined by the condition whether the rotating direction of incident polarization is the same as or opposite to the direction of the spiral rotations. Qualitative analytical expressions of the switching mechanisms and full-vectorial numerical results are presented.

OCIS codes: 230.5440, 240.6680.

[◊]Data sets associated with this article are available at http://midas.osa.org/midaspre/item/view/1043?key=a3dIM25zV3JDcDIzLg==. **Links such as "View 1" that appear in figure captions and elsewhere will launch custom data views if ISP software is present.**

1. Introduction

It is well known that the light field can transmit through subwavelength metallic aperture, the size of which is below the half wavelength, via the help of surface plasmon polaritons (SPPs) [1, 2]. Since the report of the seminal paper of extraordinary optical transmission (EOT) [3], which is an unusual enhancement of transmission efficiency compared to the conventional diffraction theory, tremendous interests have been focused on this anomalous phenomenon. Not much after the report of the EOT in two-dimensional hole arrays, it was also reported that enhanced emission of light from a single hole can be achievable if periodic corrugations are arranged around the hole at the light impinging side of metal film [4]. Interestingly enough, this paper also reported that the radiation of light from a single aperture can be designed to be highly directional if the exit side of the metal film is corrugated with periodic gratings [4]. With these studies, the interest on the manipulation of SPPs has been dramatically increased and various schemes of plasmonic beaming, focusing, and multiplexing have been reported [5–12]. The plasmonic beaming, the generation of a highly directional far-field radiating beam by the non-radiating surface plasmon sources, is one of the promising issues for applying the SPPs into several applications such as the nano-sized optical antenna [13, 14], recording [15], sensing [16, 17], or active devices [18] beyond the diffraction limit. Plasmonic beaming was firstly demonstrated by using the “bull’s eye” structure [4], which is composed of a small metallic hole surrounded by several periods of concentric annular grating corrugations. Such grating structures can efficiently convert the near-field SPP energy to the far-field radiations, since their periods are designed to compensate the momentum mismatch between the SPP mode and the radiation mode. Detailed research has been made to ascertain the relation between the grating periods and the radiation angle, leading to some novel devices such as the off-axial plasmonic beaming with asymmetric gratings [5], beam focusing with chirped gratings [6], and multiple bundle beaming [7]. More

recently, a tunable directional plasmonic beaming was proposed by using subwavelength metal-dielectric composite gratings arranged around a metal nanoslit [8]. In this structure, a thin metallic layer deposited on the dielectric structure is used to suppress side-lobes of the diffracted beam and it is shown that the beaming angle of the structure can be modified by changing the effective refractive index of the grating layer for a fixed grating period. Although not covered in this paper, for the completeness of this brief review of plasmonic beaming, we want to note here that the plasmonic beaming or focusing can also be achieved by using the array of subwavelength metallic slits [9–11]. In this case, plasmonic beam is manipulated by the appropriate phase distribution formed by tuning the metal slit thickness or slit width.

On the other side, there have been lots of studies on the generation of plasmonic hot spot or vortex field on the metal surface, which is often referred to as plasmonic lens [19]. These vortex patterns originate from the interferences of the SPPs excited at the metal slits. Recent results demonstrated that the polarization state of incident field plays an important role in the generation pattern of plasmonic field on the metal surface, such as a generation of concentric hot spot by using radially polarized light [20] or synthesis of vortex field by using circularly polarized light [21, 22]. Moreover, it has been proved that the dynamic switching of plasmonic vortex state can be achieved by changing the polarization state of incident field impinged on the plasmonic vortex lens [21].

In this paper, we propose and investigate a novel method for dynamic switching of plasmonic beam. The principle of switching mechanism is based on the change of the orbital angular momentum of the plasmonic beam. The beam with a spirally rotating field profile along the propagating axis is referred to as the vortex beam. In general, it is well-known that such vortex beam has its own angular orbital number, which is often referred to as the topological

charge number [21]. Since the characteristics of plasmonic vortex are strongly subject to the topological charge number, switching of vortex state can be achieved by changing the orbital angular momentum or polarization state of incident light.

This paper is organized as follows. In section 2, the detailed explanation of the principle of the plasmonic vortex beaming will be provided. Especially, the explicit differences in mechanisms between the plasmonic vortex lens demonstrated in Ref. [21] and the plasmonic beam generation proposed here will be clarified. The numerical results of various kinds of plasmonic beaming such as bull's eye structure and a double spiral bull's eye structure will be demonstrated in section 3. The numerical evidences of dynamic switching characteristics of plasmonic vortex beaming with double spiral bull's eye structure will also be investigated in that section. Finally, the conclusions with some suggestions on the applications of the proposed device will be presented in section 4.

2. Basic principle of the plasmonic vortex and vortex beam generation

In this section, we will discuss the physical insights of plasmonic beam generation and their switching method. The main idea of our switching mechanism is based on the utilizations of the topological charge number of vortex beam. Before going further into the concept of topological charge, we will briefly review the principles laid on the plasmonic hot spot generations in plasmonic lens [21] and the on-axis beaming. Figure 1 illustrates simple diagrams for explaining the important difference between plasmonic hot spot and beam generation. To be specific, Fig. 1(a) shows the structure for generating near field surface plasmon hot spot on the metal surface, which is used in references [20–22]. In this case, the backside-illuminated plane wave is coupled to the metal-insulator-metal (MIM) mode inside the narrow metal slit patterned on the substrate. Throughout this paper we assumed that the slit width is in subwavelength scale and the only

guided mode in MIM waveguide is fundamental hybrid plasmonic mode whose parity is symmetric with respect to the E_x field [23]. The exit-side of the metal slit can be regarded as a local capacitor so that it accumulates the surface electron of the upper side of metal substrate [24]. The wavevectors of SPPs generated from each side of a single slit have opposite directions to each other, whereas the directions of surface charge flow and hence the direction of tangential electromagnetic field which are parallel to metal surface (E_x, H_y) are in the same direction. From the Maxwell's equation, the relation between the vertical (E_z) and the tangential (E_x) electric field at the metal surface can be expressed as $E_z = \left(jk_{SPP} / \kappa_{media} \right) E_x$, where k_{SPP} is the wavenumber of SPPs and κ_{media} is the attenuation factor into the medium (metal or air). Therefore, for the counter-propagating SPPs, the directions of vertical component of the electric field are anti-parallel. By this mechanism, when two SPPs generated from different slits are interfering each other, the electric field perpendicular to the metal surface (E_z) destructively interferes at the middle point of two metal slits and the electric field parallel to metal surface (E_x) constructively interferes as shown in Fig. 1(a). Since the prominent component of electric field in SPPs is vertical one (E_z), a bright hot spot at the center of two MIM waveguide (or plasmonic lens pattern) can be obtained by the constructive interference of the E_z field. Therefore, we should consider the π-phase shift between two opposite directional SPPs [25].

However, if the focus of our interest is related to the far field beaming via the radiative coupling of SPPs by gratings, the efficient beaming condition is quite different from the previous case and it follows the mechanism shown in Fig. 1(b). The surface plasmon generated from single slit or hole is similar to the case of Fig. 1(a), which means that the π-phase shift between two directional SPPs still remains. However, this π-phase shift is compensated when they are

eventually coupled to the diffractive far field, since another π-phase shift occurs when the SPPs are coupled to the diffracted field by the gratings. This can be simply explained by the reciprocal characteristic of the grating. As depicted in Fig. 1(c), when normally incident plane wave is illuminated to the same grating structure as used in Fig. 1(b), SPPs are generated to the both side of the grating ends. At the same phase, it is easy to suppose that the electric field parallel to metal surface should be in the same direction for the both sides of excited SPPs, since it is strongly dependent to the direction of incident field at that phase condition. Therefore, the SPPs generated at the right and the left ends of the structure have the same direction of the E_x field; they have the same phase, whereas they have the opposite direction of propagation. This means that the π-phase shift is generated between both SPPs shown in Fig. 1(c), and finally we could know that this π-phase shift also occurs in Fig. 1(b) by the reciprocity.

These explanations show that the geometrical π-phase shift in plasmonic lens structures for hot spot generation is not necessary for plasmonic beaming cases. Moreover, the dominant field component for the plasmonic beaming is the tangential field components (E_x, E_y), whereas that for the generation of SPP hot spots or vortex is the vertical field component (E_z). Therefore, we cannot directly apply the concept of Bessel function formation and relation between topological charge number and vortex size, which was used in Ref. [21], to the plasmonic beaming structure. For example, in the plasmonic lens structures, the linearly polarized light incident to the ring-shaped nanoslit cannot generate single hot spot and circularly polarized light generates the dark spot rather than a hot spot. However, for the bull's eye structure, it is well known that both of the linearly polarized light and circularly polarized light can generate bright on-axis beaming [4].

Now, let us examine in detail the reason of these differences. Figure 2 shows the circular and spiral slit patterns used for the generation of dynamic switching of near field plasmonic hot spot and dark spot [21]. The black arrows denote the propagating directions of SPPs and red spots show the *z*-directional electric field at a fixed time. When the circularly polarized light is passing through the subwavelength slit, the phase delay caused by the evolution of the polarization state will modulate the phase of the excited SPPs. So when the circularity polarized light is illuminated to the simple circular slit pattern as in Fig. 2(a), the excited SPP has phase delay of 2π when we observe along the virtual contour inside the slit which is denoted with dashed black line. Since the E_z field directly follows the phase condition, the plasmonic vortex represented by the first order Bessel function of the first kind is generated rather than a hot spot [21]. If we want to compensate these circular phase shift, geometrical modification as shown in Fig. 2(b) can be used. It shows that the phase delay generated by circularly polarized light can be compensated by introducing additional propagation delay of SPP mode when the radius of spiral slit is increasing in the direction opposite to polarization rotating direction to make an increment of λ_{SPP} for one cycle. In this case, all the SPPs have the same phase when they reach the center point so the plasmonic hot spot is generated. On the other hand, if the direction of rotation of polarization is the same as the increasing direction of spiral slit as in Fig. 2(c), the propagation delay gives additional phase delay to the initial phase delay so the angular momentum of plasmonic vortex can be increased. These relations can be simply expressed by the topological charge relation which is given as [21]

$$l_{total} = l_{polarization} + l_{geometry}. \quad (1)$$

Here, we defined clockwise direction as a plus sign of total topological charge so that the polarization topological charge $l_{polarization}$ is defined as $l_{polarization} = +1$ for the right-handed circularly polarized (RCP) and $l_{polarization} = -1$ for the left-handed circularly polarized (LCP) light incidence [21]. In the same convention, $l_{geometry} = -1$ for the structure shown in Figs. 2(b) and (c). By Eg. (1) and structures shown in Fig. 2, the plasmonic vortex field generated by patterned slit can be simply switched by changing the incident polarization direction. It has been shown that the state $l_{total} = n$ follows the vortex pattern of the n^{th} order Bessel function [21].

However, due to the differences in phase compensation mechanism and dominant field component as we examined in Fig. 1, quite different explanation is needed for plasmonic beaming structure. In Fig. 3(a), the schematic diagram of bull's eye beaming structure is shown. The central metallic hole is surrounded by circular concentric gratings. Consider the case of the LCP light incidence. Similar to those in Fig. 2, black arrows denote the propagating wavevector. However, since the dominant field components are tangential fields, the colored arrows denote the directions of tangential electric field components. The red arrows near the gratings are the tangential electric field at specific time, and blue dashed arrows indicate those field components after $\pi/2$ phase has passed from the time of red arrows. The large arrows shown at the center are the directions of the tangential electric field of generated plasmonic beam measured above the metal surface. It should be pointed out that the phase of the tangential electric field component comprising the plasmonic beam is dependent on the *z*-coordinate. Here, for the sake of convenience, we set this phase be the same as that of the near-field electric component on the metal surface. Unlike the cases of Fig. 2, the fields generated from the left and right sides of the gratings do not make interference with those from the up and down side of the gratings since

they have orthogonal vector components to each other. Therefore, the polarization state at the center of beam is circularly polarized which has the same direction as the incident plane wave.

We can consider similar geometrical modification of gratings that we have considered with the slits as shown in Figs. 3(b) and 3(c): the spiral grating structure. In these cases, the additional phase delay is generated along the radial increase of propagation length from the center hole to the starting position of grating. The field generated from the left and right sides delayed by the phase of π due to the geometry but they are already $\pi/2$ phase faster than field are generated from up and down side due to the incident polarization. As a result, the incident LCP light is converted to the RCP light at the center of plasmon beam.

More interesting results could be obtained when the incident polarization has the same rotating directions with the spiral geometry as shown in Fig. 3(c). In this case the phase delays generated by polarization state and geometry are added to each other, so that the fields generated from the left and right sides have $3\pi/2$ phase slower than fields generated from up and down side gratings, which can be drawn like small colored arrows in Fig. 3(c). Assuming that the spiral grating geometry only affects the phase delay of propagating SPPs, we know that all the small arrows are equally contributed to the field generated at the central axis of plasmonic beam. However, the vector sum of these field components is completely cancelled to each other at any phase, so that it cannot provide beaming along the *z*-direction.

We would like to give a general remark here. Although we could apply the topological charge number analogy both to the in-plane plasmonic hot spot generations and plasmonic beamings, there are differences in working principles of them. In the first case, the condition of $l_{total} = 0$ makes all the SPPs have the same phase, resulting in the plasmonic hot spot. However, the plasmonic beaming is generated when the total topological charge has the value of $l_{total} = \pm 1$.

In the next section, we will verify the analogies developed in this section by using the full 3D simulations.

3. Three-dimensional plasmonic vortex beam modulation by changing the topological charge number

Throughout this section, all the simulations are performed with the use of rigorous coupled wave analysis method (RCWA) [26], which is a kind of Fourier modal method for computing full vector electromagnetic field problems. Before we show the effect of spiral-shaped grating, we simulate the conventional bull's eye structure for reference. In Fig. 4(a), the schematic of bull's eye structure used in RCWA simulation is shown, The free space wavelength λ, radius of hole r_{hole}, period of grating Λ, thickness of metal layer t_{metal}, thickness of dielectric grating layer t_{grating}, are set to λ = 650 nm, r_{hole} = 100 nm, Λ = 450 nm, t_{metal} = 250 nm, and t_{grating} = 400 nm, respectively. These parameters are based on the values which are optimized to the efficient generation of plasmonic beaming [27]. Figure 4(b) shows three-dimensional electric field intensity distribution of plasmonic beam generated by bull's eye structure when the incident plane wave is LCP. The full-width at half-maximum (FWHM) of the plasmonic beam, which is measured (in simulation) 6.5 μm above the grating, is obtained as 976 nm. It is clearly shown that, along the *z*-axis, the plasmonic beam is strongly formed, since this condition is related to the case of Fig. 3(a). Although the dominant field components for plasmonic beaming are the tangential components, the vectorial nature of these field components makes it difficult to illustrate the phase rotating characteristics. However, the vertical field component is scalar component and directly related to the phase characteristic [21]. Consequently, we can determine the total topological charge number of plasmonic beam from vertical electric field. Figure 4(c) shows the distribution of E_z field on the 10 μm above the grating. It is clearly shown that the

field is rotating counter-clockwise with one phase cycle, which proves that the beam has a total topological charge number of $l_{total} = +1$, as expected in Fig. 3(a). Note that the *x*-polarized light makes *x*-polarized beaming and *y*-polarized light makes *y*-polarized beaming along the *z*-axis for bull's eye structure. Since there are no artificial phase delay formed by the geometry, incident polarization is not changed by any polarization state of incident field. This means that bull's eye structure has polarization-independent beaming characteristics so we cannot use it for a polarization-dependent switching device. In Fig. 4(d), electric field intensity distribution is shown when the LCP light is illuminated into the metallic hole without the grating pattern. It is shown that the electric field transmitted from the hole without grating is exponentially decayed since the hole size is subwavelength scale.

As mentioned earlier in section 2, the polarization-dependent switchable beaming could be demonstrated by using the double spiral bull's eye structure. Figure 5(a) illustrates the proposed double spiral bull's eye structure composed of metallic hole and surrounding spiral-shaped dielectric gratings. The parameters we already defined in conventional bull's eye structure such as r_{hole}, Λ, t_{metal}, and t_{grating} are set to be the same value as those we have used in Fig. 4. Unlike the folded plasmonic vortex lens slit for the generation of near field plasmonic vortex [21], the double spiral bull's eye structure requires continuously coiled structure. This is because the periodic grating profile is needed for the diffraction to the specific angle that can generate a plasmonic beam [5]. The radius of single spiral grating continuously increases along the azimuthal angle, so that the radius of spiral grating will be provided as a function of azimuthal angle ϕ,

$$r_{spiral,i}(\phi) = r_0 + \frac{l_{geometry}\Lambda}{2\pi}(2\pi p + \phi_i - \phi) \quad (\text{i} = 1, 2, \ldots \text{n}, \ \phi_i \le \phi \le \phi_i + 2\pi p), \tag{2}$$

where n, p, $l_{geometry}$, r_0, and ϕ_i denote the total number of spiral dielectric grating, the winding number of each spiral grating, the geometrical topological charge of overall grating structure, the initial radius of spiral grating, and the initial offset of the azimuthal angle of each spiral grating, respectively. The minus sign used in the azimuthal angle term is due to the clockwise direction of spiral grating. In the simulations shown in Figs. 5 and 6, we use the parameter of $n = 2$ (double spiral structure), $p = 2.5$, $l_{geometry} = +2$ (clockwise), $r_0 = \frac{\Lambda}{2} + r_{hole}$, $\phi_1 = \frac{\pi}{2}$, and $\phi_2 = \frac{3\pi}{2}$. Although the number of spiral grating is not directly related to the geometrical topological charge, the symmetry of structure is broken if only the single spiral structure is used. This makes symmetry breaking of the coupling intensity along the circulation, which produces unwanted distortion to overall beaming characteristics. Therefore we used symmetric double spiral structure rather than single spiral to preserve the on-axis beaming.

Figure 5(b) shows the 3D electric field intensity distribution above the grating when the LCP (counter-clockwise) light is illuminated from the backside. Note that the strong beam is generated along the *z*-axis similar to the case of bull's eye structure. This can be explained by simple summation of topological charge number as explained in Eq. (1). In this case we could obtain the total topological charge of $l_{total} = +1$ since the value of $l_{polarization}$ is –1. The total topological charge of +1 can be obviously shown in Fig. 5(c), which illustrates the vertical electric field on the $z = 10$ μm plane. It is noteworthy that only one cycle of phase modulation is detected near the *z*-axis and it circulates along the *clockwise* direction, even though the incident polarization has *counter-clockwise* rotation direction. This means the double spiral grating structure successfully changes the angular momentum of the generated beam and finally changed the polarization state. Actually, we already showed that efficient on-axis beaming with circular

polarization can be generated when the total topological charge is +1 or –1, by using the bull's eye structure. We can assume that the bull's eye structure is a grating structure which has a geometrical topological charge of zero, which makes absolutely the same intensity pattern regardless of rotation direction of polarization. Therefore, when the LCP light illuminates the proposed double spiral bull's eye structure, it can efficiently generate plasmonic beam as if the RCP light illuminated the conventional bull's eye structure since they have exactly the same total topological charge number.

However, when the polarization state of incident beam is RCP (clockwise), the total topological charge number will be $l_{total} = +3$. The overall beam shape for this case is illustrated in Fig. 6(a). It shows quite different beam pattern from that shown in Fig. 5(b). Although the beams are generated above the double spiral grating structure, these beams are split into two main lobes and helically diverging along the propagation direction rather than merging along the *z*-axis. According to the explanation in section 2, we assumed that the spiral geometry only affects the phase delay mechanism, so that the field intensity pattern should have circular symmetric profile. However, there are side effects of spiral geometry such as phase discontinuity at the starting point of the spiral grating, diffracted light generation position mismatch due to the geometry, and coupling intensity mismatch due to the metallic loss difference. As a result, the circular symmetry of field intensity cannot be maintained. Nevertheless the topological charge relation is well-matched with theory and it can be viewed by the same manner used in Fig. 5(c). The *z*-directional electric field on the z = 10 μm plane for the case RCP light illumination is shown in Fig. 6(b). It shows that the field amplitude of the center point is relatively weak, and the field distribution near the center point has about three cycles of phase modulation and it also

circulates along the clockwise direction. This means the total topological charge of this beam is +3, and as expected in Fig. 3(c).

By using the polarization dependent beam characteristics of the proposed double spiral grating structure, the plasmonic beaming can be switched by changing the polarization states. To provide a clear view for the switching characteristic of the proposed structure, the *z*-directional power flow distributions on the $y = 0$ plane for the cases of LCP and RCP light illumination are compared in Figs. 7(a) and 7(b), respectively. It is clearly shown that bright spot along the *z*-axis is formed for LCP light incidence but is not shown in RCP light incidence. The on-off ratio of the proposed switchable beaming structure is obtained as 23.3 dB, which is defined as the ratio of *z*-directional time averaged power flow passing through a circular area of diameter of 976 nm located on $z = 8.5$ μm plane of the LCP incidence case divided by the RCP light incident case.

4. Conclusion

We proposed a novel type of plasmonic beaming structure which can be used for plasmonic beam switch by using the double spiral grating geometry. The beam generated from the proposed device has different angular momentum characteristics from that of the incident field due to the additional angular momentum generated by its own geometry. If the spiral direction is opposite to the polarization rotating direction, the plasmonic beam is generated with the opposite polarization direction compared to the incident polarization. However, when the spiral direction and polarization rotation have the same direction, the cancellation of the vector sum of tangential field component along the beaming axis prohibits the beam generation. These switchable beaming characteristics might be used for the various applications such as all-optical switching in nanoscale, optical sensing, and plasmonic data processing.

Acknowledgement

This work was supported by the National Research Foundation and the Ministry of Education, Science and Technology of Korea through the Creative Research Initiatives Program (Active Plasmonics Application Systems).

References

1. H. F. Ghaemi, T. Thio, D. E. Grupp, T. W. Ebbesen, and H. J. Lezec, "Surface plasmon enhance optical transmission through subwavelength holes," Phys. Rev. B. **58**, 6779–6782 (1998).
2. W. L. Barnes, A. Dereux, and T. W. Ebbesen, "Surface plasmon subwavelength optics," Nature **424**, 824–830 (2003).
3. T. W. Ebbesen, H. J. Lezec, H. F. Ghaemi, T. Thio, and P. A. Wolff, "Extraordinary optical transmission through sub-wavelength hole arrays," Nature **391**, 667–669 (1998).
4. H. J. Lezec, A. Degiron, E. Davaux, R. A. Linke, L. Martin-Moreno, F. J. Garcia-Vidal, and T. W. Ebbesen, "Beaming light from a subwavelength aperture," Science **297**, 820–822 (2002).
5. S. Kim, H. Kim, Y. Lim, and B. Lee, "Off-axis directional beaming of optical field diffracted by a single subwavelength metal slit with asymmetric dielectric surface gratings," Appl. Phys. Lett. **90**, 051113 (2007).
6. S. Kim, Y. Lim, H. Kim, J. Park, and B. Lee, "Optical beam focusing by a single subwavelength metal slit surrounded by chirped dielectric surface gratings," Appl. Phys. Lett. **92**, 013103 (2008).
7. S. Kim, Y. Lim, J. Park, and B. Lee, "Bundle beaming from multiple subwavelength slits surrounded by dielectric surface gratings," J. Lightwave Technol. **28**, 2023–2029 (2010).

8. H. Kim, J. Park, and B. Lee, “Tunable directional beaming from subwavelength metal slits with metal-dielectric composite surface gratings,” Opt. Lett. **34**, 2569–2571 (2009).
9. D. Choi, Y. Lim, S. Roh, I.-M. Lee, J. Jung, and B. Lee, “Optical beam focusing with a metal slit array arranged along a semicircular surface and its optimization by genetic algorithm,” Appl. Optics **49**, A30–A35 (2010).
10. H. F. Shi, C. T. Wang, C. L. Du, X. G. Luo, X. C. Dong, and H. T. Gao, “Beam manipulating by metallic nano-slits with variant widths,” Opt. Express **13**, 6815–6820 (2005).
11. W. M. Saj, “Light focusing on a stack of metal-insulator-metal waveguides sharp edge,” Opt. Express **17**, 13615–13623 (2009).
12. B. Lee, S. Kim, H. Kim, and Y. Lim, "The use of plasmonics in light beaming and focusing," Prog. Quant. Electron. **34**, 47–87 (2010).
13. A. G. Curto, G. Volpe, T. H. Taminiau, M. P. Kreuzer, R. Quidant, and N. F. van Hulst, “Unidirectional emission of a quantum dot coupled to a nanoantenna,” Science **329**, 930–932 (2010).
14. J. Li, A. Salandrino, and N. Engheta, “Shaping light beams in the nanometer scale: A Yagi-Uda nanoantenna in the optical domain,” Phys. Rev. B **76**, 245403 (2007).
15. P. Zijlstra, J. W. M. Chon, and M. Gu, “Five-dimensional optical recording mediated by surface plasmons in gold nanorods,” Nature **459**, 410–413 (2009).
16. B. Lee, S. Roh, and J. Park, “Current status of micro- and nano-structured optical fiber sensors,” Opt. Fiber Technol. **15**, 209–221 (2009).
17. N. Liu, M. Mesch, T. Weiss, M. Hentschel, and H. Giessen, “Infrared perfect absorber and its application as plasmonic sensor,” Nano Lett. **10**, 2342–2348 (2010).

18. J. A. Dionne, K. Diest, L. A. Sweatlock, and H. A. Atwater, "PlasMOStor: a metal-oxide-Si field effect plasmonic modulator," Nano Lett. **9**, 897–902 (2009).
19. Z. Liu, J. M. Steele, W. Srituravanich, Y. Pikus, C. Sun, and X. Zhang, "Focusing surface plasmons with a plasmonic lens," Nano Lett. **5**, 1726–1729 (2005).
20. G. M. Lerman, A. Yanai, and U. Levy, "Demonstration of nanofocusing by the use of plasmonic lens illuminated with radially polarized light," Nano Lett. **9**, 2139–2143 (2009).
21. H. Kim, J. Park, S.-W. Cho, S.-Y. Lee, M. Kang, and B. Lee, "Synthesis and dynamic switching of surface plasmon vortices with plasmonic vortex lens," Nano Lett. **10**, 529–536 (2010).
22. Y. Gorodetski, A. Niv, V. Kleiner, and E. Hasman, "Observation of the Spin-Based Plasmonic Effect in Nanoscale Structures," Phys. Rev. Lett. **101**, 043903 (2008).
23. J. H. Kang, D. S. Kim, and Q-Han Park, "Local capacitor model for plasmonic electric field enhancement," Phys. Rev. Lett. **102**, 093906 (2009).
24. J. A. Dionne, L. A. Sweatlock, H. A. Atwater, and A. Polman, "Plasmon slot waveguides: Towards chip-scale propagation with subwavelength-scale localization," Phys. Rev. B **73**, 035407 (2006).
25. H. Kim and B. Lee, "Diffractive slit patterns for focusing surface plasmon polaritons," Opt. Express **16**, 8969–8980 (2008).
26. H. Kim, I.-M. Lee, and B. Lee, "Extended scattering-matrix method for efficient full parallel implementation of rigorous coupled-wave analysis," J. Opt. Soc. Am. A **24**, 2313–2327 (2007).
27. H. Kim, J. Park, and B. Lee, "Finite-size nondiffracting beam from a subwavelength metallic hole with concentric dielectric gratings," Appl. Optics, **48**, G68-G72 (2009).

Figure captions

Fig. 1. Schematic diagrams for explaining (a) the interference of two SPP modes generated from two slits, which is used for generating near field surface plasmon hot spot, and (b) the plasmonic beam generation by using the dielectric grating. Black arrows denote the wavevector of SPPs whereas red and blue arrows denote the directions of electric fields, and (c) the coupling from plane wave to SPP mode by the dielectric grating to explain the phase shift compensation by the reciprocity of grating structure.

Fig. 2. Schematic diagrams which show the wavevector and vertical electric field profile of the SPPs that are generated from (a) the circular slit structure with LCP light incidence, and those on the spiral slit structure (b) with LCP light incidence and (c) with RCP light incidence.

Fig. 3. Schematic diagrams which show the wavevector and tangential electric field profile on (a) the bull's eye beaming structure with LCP light incidence, and on the clockwise rotating double spiral bull's eye structure (b) with LCP and (c) RCP light incidence.

Fig. 4. (a) Schematic diagram of the bull's eye configuration which used for numerical calculation. (b) Three-dimensional view of the electric field intensity distribution of bull's eye structure with LCP light incidence, ranged from 0 μm to 20 μm above the dielectric grating layer (View 1) and (c) vertical electric field (E_z) distribution on the z = 10 μm plane. (d) Three-

dimensional view of the electric field intensity distribution of single hole without the gratings (View 2).

Fig. 5. (a) Schematic diagram of the proposed double spiral bull's eye configuration which is used for numerical calculation. (b) Three-dimensional view of the electric field intensity distribution of double spiral bull's eye structure with LCP light incidence ranged from 0 μm to 20 μm above the dielectric grating layer (View 3) and (c) vertical electric field (E_z) distribution on the z = 10 μm plane.

Fig. 6. (a) Three-dimensional view of the electric field intensity distribution of double spiral bull's eye structure with RCP light incidence, ranged from 0 μm to 20 μm above the dielectric grating layer (View 4) and (b) vertical electric field (E_z) distribution on the z = 10 μm plane.

Fig. 7. Distributions of z-directional power flow of the proposed double spiral bull's eye structure on the y = 0 plane with the (a) LCP and (b) RCP light incidence. The color scales are in the same scale of normalized power both in (a) and (b).

Figure 1

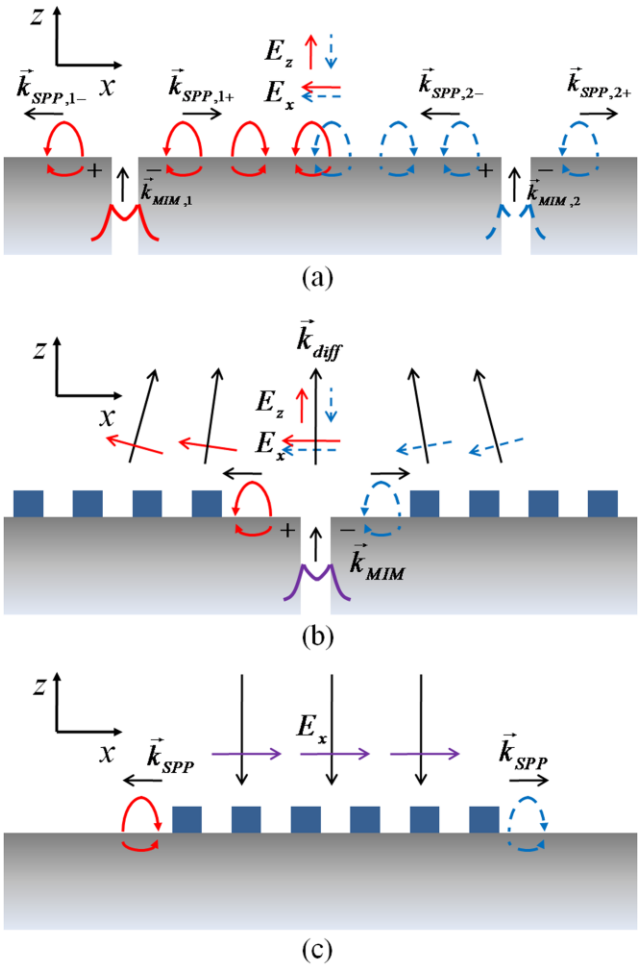
z
x
E_z
E_x
$\vec{k}_{SPP,1-}$
$\vec{k}_{SPP,1+}$
$\vec{k}_{SPP,2-}$
$\vec{k}_{SPP,2+}$
$\vec{k}_{MIM,1}$
$\vec{k}_{MIM,2}$
(a)
$\vec{k}_{diff}$
$\vec{k}_{MIM}$
(b)
$\vec{k}_{SPP}$
(c)

Figure 2

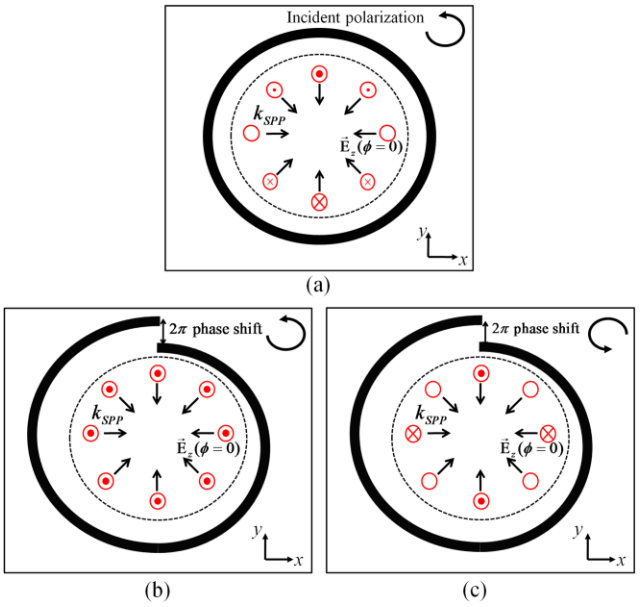
Incident polarization
k_{SPP}
$\vec{E}_z(\phi=0)$
y
x
(a)
2π phase shift
k_{SPP}
$\vec{E}_z(\phi=0)$
y
x
(b)
2π phase shift
k_{SPP}
$\vec{E}_z(\phi=0)$
y
x
(c)

Figure 3

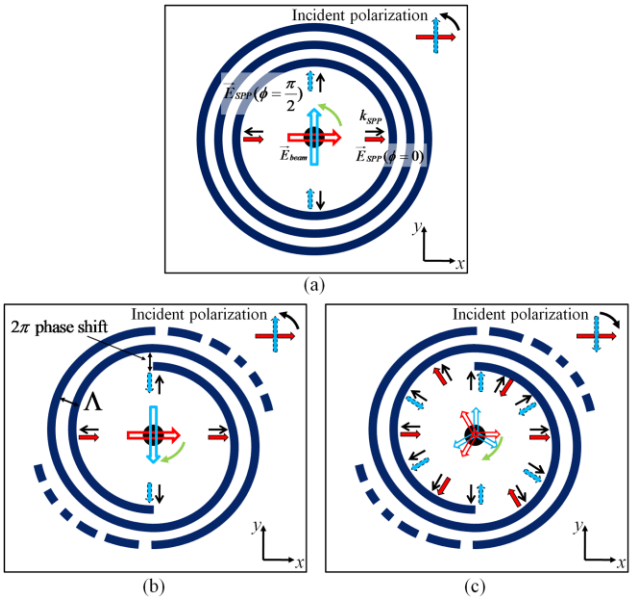
Incident polarization
$\vec{E}_{SPP}(\phi=\frac{\pi}{2})$
k_{SPP}
$\vec{E}_{beam}$
$\vec{E}_{SPP}(\phi=0)$
y
x
(a)
Incident polarization
2π phase shift
Λ
y
x
(b)
Incident polarization
y
x
(c)

Figure 4

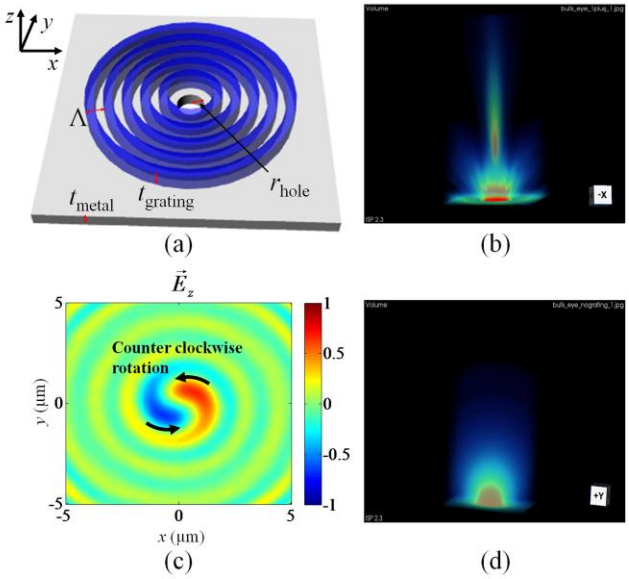
z
y
x
Λ
t_{metal}
$t_{grating}$
r_{hole}
(a)
(b)
$\vec{E}_z$
Counter clockwise rotation
y (μm)
x (μm)
5
0
-5
1
0.5
0
-0.5
-1
(c)
(d)

Figure 5

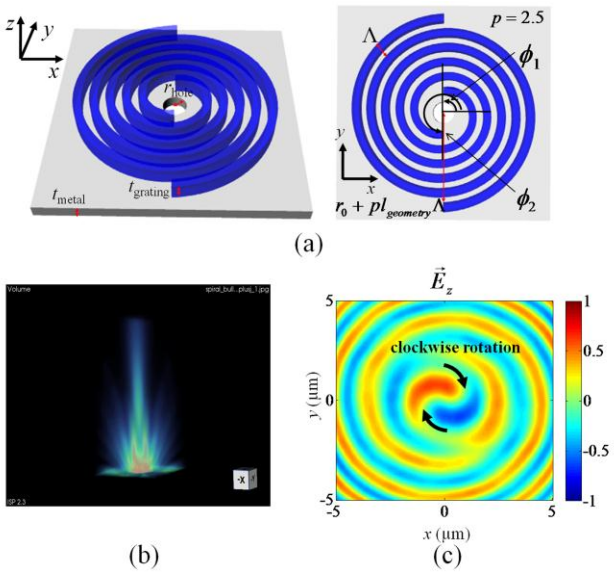
z
y
x
r_{hole}
t_{metal}
$t_{grating}$
$p = 2.5$
Λ
ϕ_1
ϕ_2
$r_0 + pl_{geometry}\Lambda$
(a)
Volume
(b)
$\vec{E}_z$
clockwise rotation
y (μm)
x (μm)
5
0
-5
1
0.5
0
-0.5
-1
(c)

Figure 6

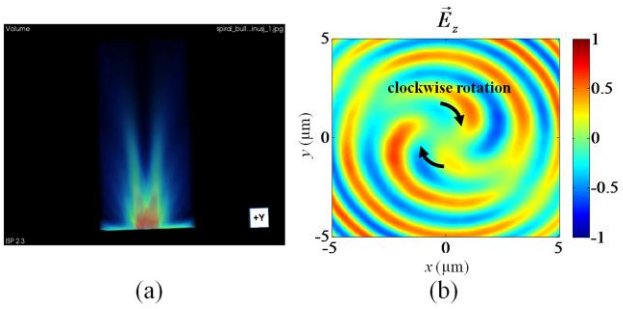

(a) (b)

Figure 7

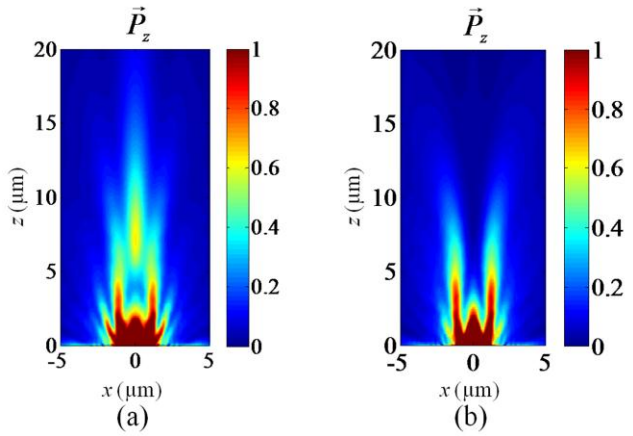
$\vec{P}_z$
20
15
10
5
0
z (μm)
-5
0
5
x (μm)
1
0.8
0.6
0.4
0.2
0
(a)
$\vec{P}_z$
20
15
10
5
0
z (μm)
-5
0
5
x (μm)
1
0.8
0.6
0.4
0.2
0
(b)